Adaptive Momentum Distribution Jitter Control for a Micro-Satellite

Hao Wang,* Lu Chen† and Zhonghe Jin‡
Zhejiang University, Hangzhou, Zhejiang, China, 310027

John L. Crassidis§
University at Buffalo, State University of New York, Amherst, New York, 14260-4400

I. Introduction

The proliferation of micro-satellites has increased the requirements for their attitude control systems [1–3]. The development of advanced reaction wheel technology makes a high-precision attitude control system possible [4, 5]. Reaction wheel assemblies (RWAs), used as an actuator for a satellite, are treated as a black box nominally for missions that do not have tight pointing requirements. In other words, the RWAs are always considered as an ideal unit that can produce the needed control torque accurately without considering their jitter or other disturbances. For large satellites, the vibration of the RWAs are usually regarded as a reason for image quality degradation [6–9]. But they do not significantly affect the overall satellite dynamic behavior. However, the moment of inertia of most micro-satellites is much smaller than larger satellites, and the jitter from RWAs can substantially affect the control accuracy. So the disturbances caused by RWA jitter may not be able to be ignored in general for micro-satellites.

The control methods for micro-satellites with RWs are nearly identical to those applied to large satellites. For example, in [10] a proportional-derivative (PD) controller, a global linear controller, a Lyapunov controller and a sliding mode controller (SMC) are compared to one another through several simulations. Some CubeSats have used proportional-integral-derivative attitude control laws in actual practice, e.g. see the 6U CubeSat in [11] and the 27U CubeSat in [12]. A constrained rate and torque feedback controller on the Bevo-2 satllite is developed in [13]. A smooth time-invariant wheel rate command, based on angular momentum balance considerations, is developed in [14]. In [15] an adaptive attitude controller in the presence of actuator faults is developed for the UKube-1 CubeSat. These above control methods use RWAs as the main attitude control device, but the disturbances introduced by the jitter of RWAs are seldom considered.

RWA jitter is usually handled by vibration isolation technology rather than by means of direct control action. Magnetic actuators can be used to reduce the torque required by the RWAs, thus enabling satellites to operate their RWs at a slower rotation speed for jitter reduction, e.g. see the Nano-JASMINE satellite [16]. However, magnetic control

*Associate Professor, Micro-Satellite Research Center, School of Aeronautics and Astronautics. Email: roger@zju.edu.cn.
†Graduate Student, Micro-Satellite Research Center, School of Aeronautics and Astronautics. Email: lynlur@163.com.
‡Professor, Micro-Satellite Research Center, School of Aeronautics and Astronautics. Email: jinzh@zju.edu.cn.
§Samuel P. Capen Chair Professor, Department of Mechanical & Aerospace Engineering. Email: johnc@buffalo.edu. Fellow AIAA.

devices require a specific installation configuration, which may be problematic for small satellites. Even though there are many research studies on RW models with jitter effects, it is still rare to implement these models into the entire control loop.

In this paper, an adaptive moment distribution control logic is proposed for a micro-satellite with RWA jitter disturbances. Specifically, an adjustment in the allocation of the attitude control torques is made according to the current speed of each RW. Since the RWA vibration torque is proportional to the wheel speed, an upper limit on the wheel speed is set to determine wheel acceleration and deceleration. Prejudgments are made before each control execution, so that the wheel speeds can be limited within a reasonable range, thus reducing RWA jitter interference. Combined with the anti-interference ability in a SMC design, the attitude accuracy of micro-satellite can be improved significantly. The approach presented in this paper uses a RWA as the only kind of actuator, and it can be implemented in multi-RW systems.

The major contribution of this paper is that the RWA jitter problem is addressed within the entire micro-satellite attitude control system. First, a micro-satellite attitude control system based on fully-coupled RWA jitter model is developed. A wheel speed feedback state machine controller is designed to assign the torque of each wheel, thus avoiding excessive jitter. Then, an adaptive moment distribution controller, which is based on parameters of the RWA onboard on the ZDPS-2 satellite, is developed and simulated. Based on both a PD controller and a SMC controller, an adaptive moment distribution control law is developed. The influence of the RWA jitter disturbance is reduced dramatically, and the control accuracy is improved by orders in magnitude.

The paper is organized as follows. In Sec. II, the RWA jitter model for the spacecraft attitude dynamics is introduced, and a control block diagram containing RWA jitter is proposed. In Sec. III, with the fully-coupled dynamical jitter model, two controllers including the traditional PD controller and SMC controller are applied. Based on the PD controller and the SMC controller, the principle of the adaptive moment distribution logic is introduced, and its asymptotic stability properties are analyzed in detail. In Sec. IV, the ZDPS-2 satellite parameters are substituted into the model. Simulations and comparisons of the controllability properties among different controllers are highlighted. Concluding remarks are made in Sec. V.

II. Control Block Diagram and RWA Jitter Model

A. Control Block Diagram

The overall control block diagram is shown in Fig. 1. The attitude control block diagram consists of a micro-satellite, sensors, a controller and actuators. The micro-satellite's attitude quaternion $\mathbf{Q}_0$ is provided by the attitude determination system. The vector part of the quaternion, denoted by $\mathbf{q}_e$, and the angular rate $\boldsymbol{\omega}_{B/N}$ are sent to the controller. The controller outputs the commanded wheel torque $\mathbf{U}_s$. Then according to the command, the actuator generates the

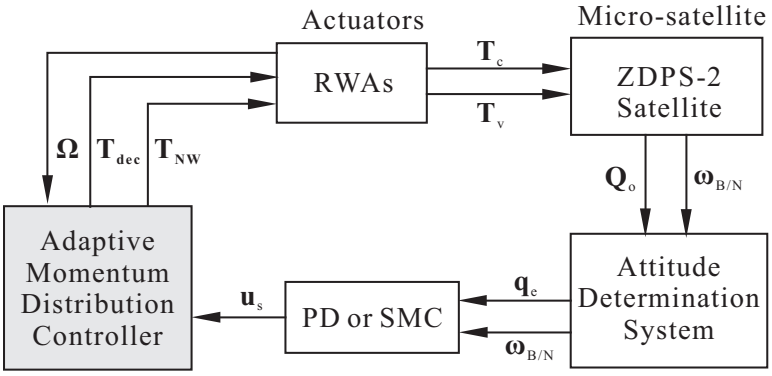

Fig. 1 Micro-satellite attitude control block diagram.

corresponding torque $\mathbf{T}_c$ acting on the micro-satellite. The vector $\mathbf{\Omega}$ is made up of the individual wheel speeds. Also, $\mathbf{T}_{dec}$ is the deceleration torque, and $\mathbf{T}_{NW}$ is the torque corresponding to the “normal" wheels; both terms are explained in detail later.

The above description is a typical model of a satellite attitude control system. However, in actual practice, the torque produced from RWA jitter $\mathbf{T}_v$ is also applied to the micro-satellite, which can also affect the satellite's attitude. The focus of this paper is designing a control scheme to deal with RW jitter effects. First, the actuators' impact on the micro-satellite will be analyzed. Sensors for the attitude determination system are not the key point of the paper, and thus will not be discussed here.

B. RWA Jitter Fully-Coupled Model

Normally, when designing a satellite attitude controller, the RWs are considered as ideal actuators, which means they can produce the torque without vibration. A general RW consists of a rotating flywheel mounted on ball bearings encased in a housing and driven by an internal brushless DC motor [17]. Due to the flexible mechanical effects of the RW structure and the limited production accuracy, it is always accompanied by vibration when the wheel spins. In [18, 19] a steady-state empirical model and a nonlinear analytical model are presented, showing the relationship between vibration and wheel speed. The imbalance of the wheel is the main cause of vibration, which is illustrated in Fig. 2 [20].

The offset of the center of mass in the axial direction causes the static imbalance, which can be modeled as a small mass m_s placed at a radius r_s on the wheel. The misalignment between the spindle and the principal axis of the wheel results in the dynamic imbalance. It is modeled as two equal masses, m_d, placed 180° apart at a radial distance, r_d, and an axial distance, h, from the center of the wheel. According to the model including the wheel imbalance, the derived

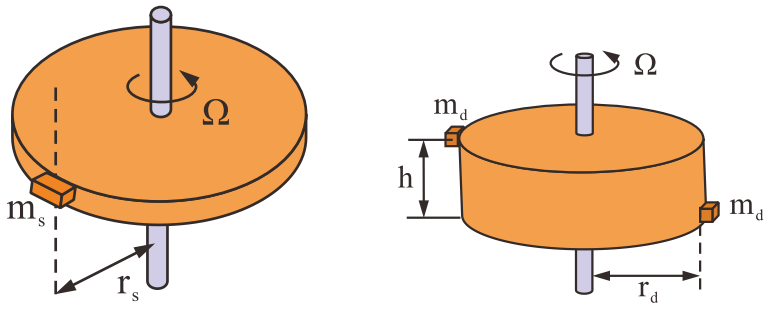

(a) Static imbalance **(b) Dynamic imbalance**

Fig. 2 Wheel imbalance modes.

solution for the force is given by [18, 19]

$$U_{\mathrm{s}} = m_{\mathrm{s}} r_{\mathrm{s}} \tag{1a}$$

$$x \equiv \frac{U_{\mathrm{s}}\Omega^2}{\beta_t}[(\Omega^2 m_{\mathrm{rw}} - k)\sin(\Omega t) + c\Omega\cos(\Omega t)] \tag{1b}$$

$$\beta_t \equiv (k - \Omega^2 m_{\mathrm{rw}})^2 + (c\Omega)^2 \tag{1c}$$

$$F_x = kx \tag{1d}$$

where U_{s} is the static imbalance, m_{rw} is the total mass of the wheel, k is a spring stiffness term, c is a damping coefficient term, and Ω is the wheel speed. It can be seen from Eq. (1) that the force F_x of the static imbalance is simply proportional to the wheel speed squared. Thus, higher wheel speeds result in greater vibration, except at the resonance point. The situation for dynamic imbalance is similar.

In recent years, many models for flywheel vibrations have been proposed, which are focused on the relationship between wheel speed and vibration. These models include a vibration model of a cantilever-configured RWA [21, 22], the dynamic mass of the wheel and the driving point acceleration of the supporting structure [23, 24], a complete vibration dynamical model of the magnetically suspended wheel with a magnetic bearing control system [25], and a RW dynamic model based upon energy [26]. According to these studies, the RWA's jitter is composed of high-order harmonics, but the impact of the fundamental frequency is the largest.

Here the model in [27] is applied, which is a generalized approach to RW imbalance modeling of a rigid hub with n RWs with a normally configured micro-sat. The fully-coupled model does not include higher-order effects, but it is reasonable to assume that the impact of the fundamental jitter is the largest disturbance. Furthermore, in the fully coupled model, the jitter effect is regarded as an internal effect rather than an external force and torque on the spacecraft. This is different from other models, but is valid in terms of conservation of energy and angular momentum. A four-wheel RWA is considered in the present work. The fully-coupled model will be briefly introduced in following.

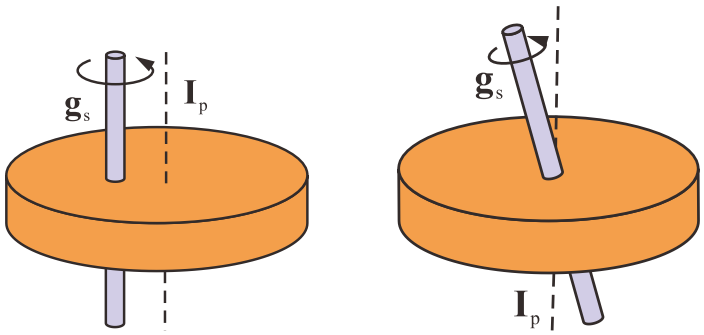

(a) Static imbalance (b) Dynamic imbalance

Fig. 3 Imbalance of a reaction wheel.

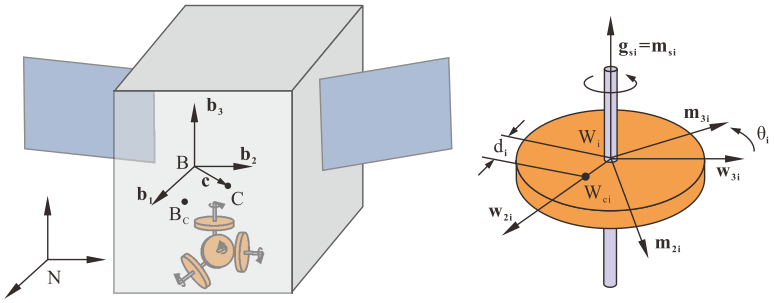

Fig. 4 Variables and reference frame definitions.

The RWA wheel imbalance is usually composed of static imbalance and dynamic imbalance. As shown in Fig. 3, static imbalance results from the offset of the center of mass of the RW ($\mathbf{I}_\mathrm{p}$) from the spin axis ($\mathbf{g}_\mathrm{s}$), and dynamic imbalance is caused by the misalignment of the wheel's principal axis ($\mathbf{I}_\mathrm{p}$) and the rotation axis ($\mathbf{g}_\mathrm{s}$). Considering this imbalance into the micro-satellite, as shown in Fig. 4, the relevant reference frames and variables are defined as follows:

1) The center of mass of the micro-satellite is labeled as point $\mathrm{B_c}$;
2) Point C is the center of mass of the micro-satellite including the RWs, and vector $\mathbf{c}$ points from B to C;
3) The body frame of the micro-satellite is B : $\{\mathbf{b}_1, \mathbf{b}_2, \mathbf{b}_3\}$, which can be oriented in any direction. Point B is the origin of the B frame that does not have to be identical to the centroid of micro-satellite;
4) The inertial frame is defined as N;
5) The RWA is composed of four RWs, and the center of mass of the i^{th} RW is labeled as W_{ci};
6) The wheel frame of the i^{th} RW is defined as W_i : $\{\mathbf{g}_{si}, \mathbf{w}_{2i}, \mathbf{w}_{3i}\}$. The vector $\mathbf{g}_{si}$ is the i^{th} RW's spin axis, the $\mathbf{w}_{2i}$ axis is perpendicular to $\mathbf{g}_{si}$ and points to $\mathbf{w}_{ci}$, and $\mathbf{w}_{3i}$ completes the triad. Point W_i is the origin of the W_i frame and can also have any location relative to point B;
7) The variable d_i is the center of mass offset of the i^{th} RW; and
8) The motor frame of the i^{th} RW is M_i : $\{\mathbf{m}_{si}, \mathbf{m}_{2i}, \mathbf{m}_{3i}\}$. The M_i frame is aligned with the W_i frame at the beginning of the simulation, and thereafter the M_i and W_i frames are offset by an angle about the $\mathbf{m}_{si}$ axis.

The equations of motion for a micro-satellite with four RWs are given by

$$I_{\text{LHS}}\dot{\omega}_{\text{B/N}} = \boldsymbol{\tau}_{\text{RHS}} \tag{2}$$

where I_{LHS} is a 3×3 matrix defined as

$$I_{\text{LHS}} = I_{\text{sc,B}} + m_{\text{sc}}\left[\tilde{\mathbf{c}}\right]\left[\tilde{\mathbf{c}}\right] + \sum_{i=1}^{4}\left\{I_{\text{rw,Wc}i}\mathbf{g}_{\text{s}i} + m_{\text{rw}i}d_i\left(\left[\tilde{\mathbf{r}}_{\text{Wc}i/\text{B}}\right] - \left[\tilde{\mathbf{c}}\right]\right)\mathbf{w}_{3i}\right\}\left(\mathbf{e}_i^T F\right) \tag{3}$$

where m_{sc} is the mass of of the satellite including the RWs and $\tilde{\mathbf{r}}_{\text{Wc}i/\text{B}}$ is location vector of the i^{th} RW. The notation $[\tilde{\cdot}]$ is used to denote the standard cross product matrix [28]. The torque vector $\boldsymbol{\tau}_{\text{RHS}}$ is given by

$$\begin{aligned}\boldsymbol{\tau}_{\text{RHS}} =& -\left[\tilde{\omega}_{\text{B/N}}\right] I_{\text{sc,B}}\,\omega_{\text{B/N}} - I'_{\text{sc,B}}\omega_{\text{B/N}} - m_{\text{sc}}\left[\tilde{\mathbf{c}}\right]\left(-2\left[\tilde{\omega}_{\text{B/N}}\right]\mathbf{c}' - \left[\tilde{\omega}_{\text{B/N}}\right]\left[\tilde{\omega}_{\text{B/N}}\right]\mathbf{c}\right)\\ &+ \sum_{i=1}^{4}\Bigg\{m_{\text{rw}i}d_i\Omega_i^2\left[\tilde{\mathbf{r}}_{\text{Wc}i/\text{B}}\right]\mathbf{w}_{2i} - I'_{\text{rw,Wc}i}\Omega_i\mathbf{g}_{\text{s}i} - \left[\tilde{\omega}_{\text{B/N}}\right]\left(I_{\text{rw,Wc}i}\Omega_i\mathbf{g}_{\text{s}i} + m_{\text{rw}i}\left[\tilde{\mathbf{r}}_{\text{Wc}i/\text{B}}\right]\mathbf{r}'_{\text{Wc}i/\text{B}}\right)\\ &- m_{\text{rw}i}d_i\Omega_i^2\left[\tilde{\mathbf{c}}\right]\mathbf{w}_{2i} - \left[I_{\text{rw,Wc}i}\mathbf{g}_{\text{s}i} + m_{\text{rw}i}d_i\left(\left[\tilde{\mathbf{r}}_{\text{Wc}i/\text{B}}\right] - \left[\tilde{\mathbf{c}}\right]\right)\mathbf{w}_{3i}\right]\left(\mathbf{e}_i^T\mathbf{v}\right)\Bigg\}\end{aligned} \tag{4}$$

where $(\cdot)'$ is used to denote the body-frame time-derivative. The matrix F is a 4×3 matrix with row components given by

$$\mathbf{f}_i^T = -\left[\left(J_{11i} + m_{\text{rw}i}d_i^2\right)\mathbf{g}_{\text{s}i}^T + J_{12i}\mathbf{w}_{2i}^T + J_{13i}\mathbf{w}_{3i}^T + \left[m_{\text{rw}i}d_i\mathbf{w}_{3i}^T\right]\left(\left[\tilde{\mathbf{c}}\right] - \left[\tilde{\mathbf{r}}_{\text{Wc}i/\text{B}}\right]\right)\right] \tag{5}$$

where the $J_{\ell ki}$ are inertia parameters. The vectors $\mathbf{e}_i$ are derived from the following 4×4 matrix:

$$E \equiv \begin{bmatrix}\mathbf{e}_1^T\\ \mathbf{e}_2^T\\ \mathbf{e}_3^T\\ \mathbf{e}_4^T\end{bmatrix} = A^{-1} \tag{6}$$

where the elements of the A matrix are given by

$$a_{ii} = J_{11i} + m_{\text{rw}i}d_i^2 - \frac{m_{\text{rw}i}^2 d_i^2}{m_{\text{sc}}} \tag{7a}$$

$$a_{ij} = -\frac{m_{\text{rw}i}d_i\mathbf{w}_{3i}^T}{m_{\text{sc}}}m_{\text{rw}j}d_j\mathbf{w}_{3j} \tag{7b}$$

The vector $\mathbf{v}$ is a 4×1 vector with elements given by

$$
\begin{aligned}
v_i = & -m_{\mathrm{rw}i} d_i \mathbf{w}_{3i}^T \left(-2 \left[\tilde{\boldsymbol{\omega}}_{\mathrm{B/N}}\right] \mathbf{c}' - \left[\tilde{\boldsymbol{\omega}}_{\mathrm{B/N}}\right] \left[\tilde{\boldsymbol{\omega}}_{\mathrm{B/N}}\right] \mathbf{c} + \frac{1}{m_{\mathrm{sc}}} \sum_{j=1; j\neq i}^{4} m_{\mathrm{rw}j} d_j \Omega_j^2 \mathbf{w}_{2j} \right) \\
& + J_{23i} \left(w_{w3i}^2 - w_{w2i}^2 \right) + w_{si} \left(J_{12i} w_{w3i} - J_{13i} w_{w2i} \right) + w_{w2i} w_{w3i} \left(J_{22i} - J_{33i} - m_{\mathrm{rw}i} d_i^2 \right) \\
& - m_{\mathrm{rw}i} d_i \mathbf{w}_{3i}^T \left[\tilde{\boldsymbol{\omega}}_{\mathrm{B/N}}\right] \left[\tilde{\boldsymbol{\omega}}_{\mathrm{B/N}}\right] \mathbf{r}_{\mathrm{W}ci/\mathrm{B}} + u_{si}
\end{aligned}
\tag{8}
$$

where u_{si} are the components of $\mathbf{u}_{\mathrm{s}}$, which is the control torque generated by all RWs. Note that the W_i frame components of $\boldsymbol{\omega}_{\mathrm{B/N}}$ are defined as:

$$
w_{si} = \mathbf{g}_{si}^T \boldsymbol{\omega}_{\mathrm{B/N}} \tag{9a}
$$

$$
w_{w2i} = \mathbf{w}_{2i}^T \boldsymbol{\omega}_{\mathrm{B/N}} \tag{9b}
$$

$$
w_{w3i} = \mathbf{w}_{3i}^T \boldsymbol{\omega}_{\mathrm{B/N}} \tag{9c}
$$

The inertia matrix of the RW in the W_i frame is defined by

$$
I_{\mathrm{rw,W}ci} = \begin{matrix} \\ \\ \\ \end{matrix}^{\mathrm{W}_i} \begin{bmatrix} J_{11i} & J_{12i} & J_{13i} \\ J_{12i} & J_{22i} & J_{23i} \\ J_{12i} & J_{23i} & J_{33i} \end{bmatrix} \tag{10}
$$

The inertia matrix of the micro-satellite can be expressed through

$$
I_{\mathrm{rw}i,\mathrm{B}} = I_{\mathrm{rw,W}ci} + m_{\mathrm{rw}i} \left[\tilde{\mathbf{r}}_{\mathrm{W}ci/\mathrm{B}}\right] \left[\tilde{\mathbf{r}}_{\mathrm{W}ci/\mathrm{B}}\right]^T \tag{11}
$$

and

$$
I_{\mathrm{sc,B}} = I_{\mathrm{hub,B}} + \sum_{i=1}^{4} I_{\mathrm{rw}i,\mathrm{B}} \tag{12}
$$

where $I_{\mathrm{hub,B}}$ is the known inertia of the wheel hub. Substituting Eqs. (3)−(12) into Eq. (2), the angular acceleration $\dot{\boldsymbol{\omega}}_{\mathrm{B/N}}$ of the micro-satellite can be solved, and then the angular rate can be obtained by integration. When $\dot{\boldsymbol{\omega}}_{\mathrm{B/N}}$ is

determined, then the angular acceleration $\dot{\Omega}_i$ and the angular rate Ω_i of each RW can be obtained through

$$\begin{bmatrix} \dot{\Omega}_1 \\ \dot{\Omega}_2 \\ \dot{\Omega}_3 \\ \dot{\Omega}_4 \end{bmatrix} = E\,F\dot{\omega}_{\mathrm{B/N}} + E\mathbf{v} \tag{13}$$

Equation (4) is the equivalent torque on the rotational motion due to the fully-coupled model. One of its terms can be seen as the static imbalance torque, given by

$$\mathbf{T}_s = \sum_{i=1}^{4} m_{\mathrm{rw}i} d_i \Omega_i^2 \left[\tilde{\mathbf{r}}_{\mathrm{W}ci/\mathrm{B}}\right] \mathbf{w}_{2i} \tag{14}$$

This is an internal torque due to the center of mass offset of the RW. The dynamic imbalance term is given by

$$\mathbf{T}_d = \sum_{i=1}^{4} I'_{\mathrm{rw,W}ci} \Omega_i \mathbf{g}_{\mathrm{s}i} \tag{15}$$

From Eqs. (14) and (15), the jitter caused from the RWs at different wheel speeds to the control loop can be found in order to observe their effect.

III. Reducing RWA Jitter on a Micro-Satellite's Control System

In this section the effect of RW on the control system of a micro-satellite is shown, and then a jitter mitigation scheme is develop. First, an adaptive moment distribution control logic, which is robust to RWA jitter, is also presented to make ensure the wheel speeds have boundaries. Then, an SMC design is used to deal with bounded disturbances. A PD controller is also presented as a comparison. Based on the PD controller and SMC, the principle of the adaptive moment distribution logic is stated in detail.

A. PD Controller

The PD controller is given by

$$\mathbf{u}_s = -K_p \mathbf{q}_e - K_d \omega_{\mathrm{B/N}} \tag{16}$$

where $\mathbf{u}_s$ is the torque required for micro-satellite attitude adjustment, $\mathbf{q}_e$ is a vector part of the quaternion, and K_p and K_d are the matrix gain matrices of the controller. The controller is a standard PD controller; details of the derivation can be found in [29, 30].

B. Sliding Mode Controller

To maintain the actuator torques within the limits of the micro-satellite hardware, a globally stable SMC algorithm is used in the presence of control input saturation and external disturbances. The SMC design is based on the use of the following sliding surface:

$$\mathbf{s} = \boldsymbol{\omega}_{\mathrm{B/N}} + k_s \mathbf{q}_e \tag{17}$$

The vector part of the quaternion $\mathbf{q}_e$, and the micro-satellite body angular rate $\boldsymbol{\omega}_{\mathrm{B/N}}$ are used as feedback terms for the controller. The control law then becomes [31]:

$$\mathbf{u}_s = -\begin{bmatrix} \mathrm{sgn}(s_1) & 0 & 0 \\ 0 & \mathrm{sgn}(s_2) & 0 \\ 0 & 0 & \mathrm{sgn}(s_3) \end{bmatrix} \begin{bmatrix} u_m \\ u_m \\ u_m \end{bmatrix} \tag{18a}$$

$$\dot{k}_{\mathrm{s}} = -\gamma_{\mathrm{s}} u_m \sum_{i=1}^{3} \left[\mathrm{sgn}(k_{\mathrm{s}}) \left| q_{ei} \right| + q_{ei} \mathrm{sgn}(s_i) \right] \tag{18b}$$

The term k_{s} is used to achieve relative weighting between $\mathbf{q}_e(t)$ and $\boldsymbol{\omega}_{\mathrm{B/N}}(t)$. This strategy attempts to stabilize both $\mathbf{q}_e(t)$ and $\boldsymbol{\omega}_{\mathrm{B/N}}(t)$ simultaneously from any initial condition. The scalar $\gamma_{\mathrm{s}} > 0$ is a adaptive gain, which does not affect the stability analysis, and can be chosen to improve the performance. The term u_m is the control torque bound. This control algorithm can guarantee the stability with $u_m > z$, where z denotes a value of the assumed external disturbances. When only consider environmental disturbances, such as gravitational torque, aerodynamic drag torque, solar radiation torque and magnetic torque, the SMC can achieve stable control. However, when the wheel jitter is considered, the interference may exceed the maximum control torque, resulting in instability of the micro-satellite attitude. Therefore, it is necessary to pre-control the RWA jitter. A comparison of the control effects will be given in the simulations.

C. Adaptive Moment Distribution Control Logic

As mentioned previously, the force and torque of a RWA's jitter are proportional to wheel speed squared, except for the resonance point associated with RW modes. Therefore, it seems better to generate the target torques with a lower wheel speed. But there is a tradeoff between lower wheel speed limit and output torque, because the RWA would be saturated frequently with a lower speed limit. The wheel speeds are used as a feedback to reassign the command torque. For a RWA consisting of four RWs, the i^{th} wheel spin axis unit vector is defined as $\mathbf{g}_{si}$ in the micro-satellite body B frame:

$$\mathbf{g}_{si} = \begin{bmatrix} x_{si} & y_{si} & z_{si} \end{bmatrix}^T \tag{19}$$

The 3×4 matrix of RWA's alignment, with its row elements defined as $\mathbf{g}_{si}$, is given by

$$G_{\mathrm{s}} = \begin{bmatrix} \mathbf{g}_{\mathrm{s}1} & \mathbf{g}_{\mathrm{s}2} & \mathbf{g}_{\mathrm{s}3} & \mathbf{g}_{\mathrm{s}4} \end{bmatrix} \tag{20}$$

The vector of wheel speeds (in rpm) in the inertial N frame is given by

$$\mathbf{\Omega} = \begin{bmatrix} \Omega_1 & \Omega_2 & \Omega_3 & \Omega_4 \end{bmatrix}^T \tag{21}$$

The amplitude of the RW jitter will be enlarged at the static imbalance resonance point, so this point is good to be set as the upper wheel speed limit of the RW to avoid excessive jitter. Here Ω_{U}, which is lower than the resonance point, is selected as the wheel speed limit. At this moment, the RW jitter torque is less than the maximum torque that the RWs could provide. Now suppose there are wheels that exceed the upper limit at some time. These wheels are called "over-speed" wheels, while the others are called normal wheels. For the over-speed group, it is necessary to apply a deceleration torque $\mathbf{T}_{\mathrm{dec}i}$ on each wheel:

$$\mathbf{T}_{\mathrm{dec}i} = -\mathrm{sgn}(\Omega_i) \cdot \mathrm{T}_{\mathrm{dec}} \cdot \mathbf{g}_{si} \tag{22}$$

where $\mathrm{T}_{\mathrm{dec}}$ is the modulus of the deceleration torque, and Ω_i is the speed of i^{th} wheel that exceeds the upper limit Ω_{U}. For the normal group, besides producing the required control torques of micro-satellite attitude, they are also required to compensate for the sum of the decelerating torque $\mathbf{T}_{\mathrm{dec}i}$. As a result, the torque $\mathbf{T}_{\mathrm{N}}$ that normal wheels should provide is

$$\mathbf{T}_{\mathrm{N}} = \mathbf{u}_{\mathrm{s}} - \sum_{i=1}^{m} \mathbf{T}_{\mathrm{dec}i} \tag{23}$$

where m is the number of over-speed wheels.

The normal wheels' mounting matrix can be expressed as a $3 \times (4 - m)$ matrix:

$$G_{\mathrm{s(4-m)}} = \begin{bmatrix} \mathbf{g}_{\mathrm{s}1} & \mathbf{g}_{\mathrm{s}2} & \cdots & \mathbf{g}_{\mathrm{s}(4-m)} \end{bmatrix} \tag{24}$$

The torque is assigned by the pseudo-inverse method:

$$\mathbf{T}_{\mathrm{NW}} = G_{\mathrm{s}(4-m)}^T \left(G_{\mathrm{s}(4-m)} G_{\mathrm{s}(4-m)}^T \right)^{-1} \mathbf{T}_{\mathrm{N}} \tag{25}$$

The torque $\mathbf{T}_{\mathrm{NW}}$ can be expressed as an $(4 - m) \times 1$ vector, corresponding to the normal wheels in the mounting matrix.

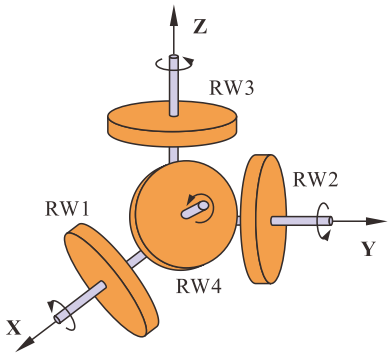

Fig. 5 Configuration of the RWA.

The resultant torque of the RWA is then

$$\mathbf{u}_{\mathrm{s}} = \left[G_{\mathrm{s}(4-m)}\right] \mathbf{T}_{\mathrm{NW}} + \sum_{i=1}^{m} \mathbf{T}_{\mathrm{dec}i} \tag{26}$$

This control logic can produce a satellite attitude control torque, and reduce the high wheel speed at the same time. It should be noted, however, that the number of normal wheels must not be smaller than three, and their orientation should not be in the same plane.

D. State Machine Translation

The method of state machine translation is chosen to complete the control process, which involves a three-orthogonal and one-oblique configuration as the overall system. To avoid speed fluctuations in a wheel when approaching the upper limit, the over-speed wheel speed is applied to a deceleration torque until its speed is much lower than the speed limit. The configuration of the RWA is shown in Fig. 5. Reaction wheels are along the X, Y and Z axes, and the oblique axis respectively, and are numbered as RW1, RW2, RW3 and RW4. According to the over-speed of the RWs, the running state of the RWA can be divided into five types, as shown in Table 1.

When a wheel or multiple ones exceed a speed limit at a certain moment, a priority in the wheel speed is required to determine which wheel should be decelerated. It obviously depends on the mounting position of the wheel relative to the micro-satellite. For example, as is well-known, to maintain conservation of angular momentum, if RW4's speed changes, the other three wheel speeds also need to change. Thus, RW4 has the greatest priority and will be constrained preferentially. Then the farther the centroid of the wheel is from the body center of the micro-satellite, the greater the jitter affects the attitude of the micro-satellite. Therefore, in the actual decision, the priority of over-speed judgment is set from far to near. Following this priority, the translation of the status machine is shown in Fig. 6. State 5 is the initial stage, in which all wheel speeds are under the upper limit. When there is an over-speed wheel, the status of the RWA would convert to other possible states according to the priority level. If there are no other wheels running at an

Table 1 Running state of the RWA

State	Over-Speed Wheel	$G_{s(4-m)}$
1	RW1	${}^{B}\begin{bmatrix} 0 & 0 & -0.5774 \\ -1 & 0 & -0.5774 \\ 0 & -1 & -0.5774 \end{bmatrix}$
2	RW2	${}^{B}\begin{bmatrix} -1 & 0 & -0.5774 \\ 0 & 0 & -0.5774 \\ 0 & -1 & -0.5774 \end{bmatrix}$
3	RW3	${}^{B}\begin{bmatrix} -1 & 0 & -0.5774 \\ 0 & -1 & -0.5774 \\ 0 & 0 & -0.5774 \end{bmatrix}$
4	RW4	${}^{B}\begin{bmatrix} -1 & 0 & 0 \\ 0 & -1 & 0 \\ 0 & 0 & -1 \end{bmatrix}$
5	None	${}^{B}\begin{bmatrix} -1 & 0 & 0 & -0.5774 \\ 0 & -1 & 0 & -0.5774 \\ 0 & 0 & -1 & -0.5774 \end{bmatrix}$

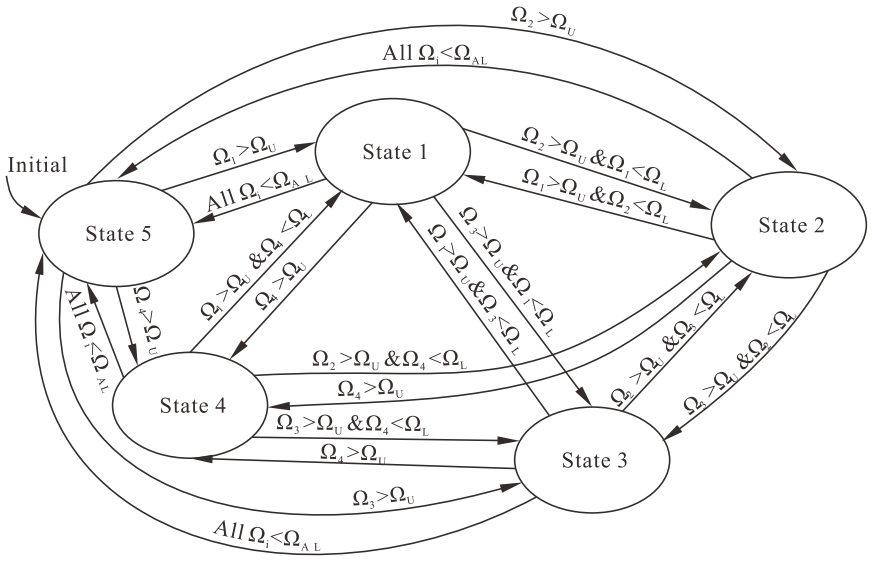

Fig. 6 State machine translation.

excessive speed, then the RWA will remain in its current state and slow down the current wheel speed. The RWA will stay in a certain state until the wheel speed drops to a preset speed Ω_{AL}. Once all the wheels speeds are below Ω_{AL}, the RWA will jump back to state 5.

In summary, the PD controller or SMC controller outputs the torque command according to the micro-satellite's current attitude. Then, the adaptive moment distribution control logic divides the wheels into two groups to generate required torques while decelerating the over-speed wheel. Finally, the micro-satellite attitude is controlled at lower wheel speeds, which helps mitigate the interference due to RWA jitter.

IV. Simulations

Real parameters from ZDPS-2, which is a micro-satellite launched on Sept. 22nd, 2015, are used in the simulations. The RWA jitter is simulated based on the fully-coupled RWA model and the real actual RWA configuration used on ZDPS-2. A PD control algorithm, which is also used on the ZDPS-2, is applied to reduce the jitter effect. In addition, the adaptive SMC is also utilized to reduce the jitter as a comparison. The simulation parameters used are given in Table 2, where C.O.M. denotes center of mass.

To focus strictly on the jitter's effect on the control system, it is assumed that true values of the satellite's attitude is given during the simulations. That is, sensor errors are not considered. The RWA is considered as an ideal component firstly, i.e. with no jitter effects. As shown in Fig. 7, the control result of the micro-satellite's attitude error is almost zero when the RWA is ideal. However, under the same conditions the attitude error can reach 6° when the RWA's jitter is considered in the control loop. Clearly, the RWA jitter can indeed affect the attitude of the micro-satellite. The fully-coupled micro-satellite dynamical model is used, and the traditional PD controller is applied, which is close to the

Table 2 Parameters used in the simulations

Parameter	Notation	Value	Units
Number of Reaction Wheels	n	4	–
Satellite Mass	m_{sc}	17	kg
Orbital Angular Velocity	$\omega_{\text{O/N}}$	0.0011	rad/s
Initial Attitude Angles	θ_{I}	$[\ 0.65 \quad -0.17 \quad -0.2\ ]^T$	deg
Wheel Mass	m_{rw}	0.01	kg
Hub Inertia Tensor	$I_{\text{hub/B}}$	$^{\text{B}}\begin{bmatrix} 1.68 & 0.1045\times10^{-4} & -0.84\times10^{-5} \\ 0.1045\times10^{-4} & 1.0798 & 1\times10^{-8} \\ -0.84\times10^{-5} & 1\times10^{-8} & 1.0798 \end{bmatrix}$	$\text{kg}\cdot\text{m}^2$
Hub C.O.M. Location	$\mathbf{r}_{\text{Bc/B}}$	$^{\text{B}}\begin{bmatrix} 5 & 5 & 10 \end{bmatrix}^T$	mm
Wheel Alignment Matrix	G_{s}	$^{\text{B}}\begin{bmatrix} -1 & 0 & 0 & -0.5774 \\ 0 & -1 & 0 & -0.5774 \\ 0 & 0 & -1 & -0.5774 \end{bmatrix}$	–
Wheel Static Imbalance	U_{s}	3.5×10^{-8}	$\text{kg}\cdot\text{m}$
Wheel Dynamic Imbalance	U_{d}	1.52×10^{-10}	$\text{kg}\cdot\text{m}^2$
Wheel C.O.M. Offset	d	3.5	μm
Wheel Inertia Tensor	$I_{\text{rw/Wc}}$	$^{\text{W}}\begin{bmatrix} 1.782\times10^{-6} & 0 & 1.52\times10^{-10} \\ 0 & 0.912\times10^{-6} & 0 \\ 1.52\times10^{-10} & 0 & 0.912\times10^{-6} \end{bmatrix}$	$\text{kg}\cdot\text{m}^2$
Wheel 1 Location Vector	$\mathbf{r}_{\text{W1/B}}$	$^{\text{B}}\begin{bmatrix} 54.50 & 94.19 & 16.69 \end{bmatrix}^T$	mm
Wheel 2 Location Vector	$\mathbf{r}_{\text{W2/B}}$	$^{\text{B}}\begin{bmatrix} 90.34 & 58.50 & 16.06 \end{bmatrix}^T$	mm
Wheel 3 Location Vector	$\mathbf{r}_{\text{W3/B}}$	$^{\text{B}}\begin{bmatrix} 90.40 & 93.86 & -19.5 \end{bmatrix}^T$	mm
Wheel 4 Location Vector	$\mathbf{r}_{\text{W4/B}}$	$^{\text{B}}\begin{bmatrix} 69.57 & 73.08 & -4.91 \end{bmatrix}^T$	mm
Initial Wheel Speeds	$\boldsymbol{\Omega}$	$\begin{bmatrix} -534 & -86 & 232 & 2124 \end{bmatrix}^T$	rpm
Deceleration Torque	T_{dec}	7×10^{-5}	$\text{N}\cdot\text{m}$
Target Attitude Angles	$\boldsymbol{\theta}_{\text{T}}$	$[\ 0 \quad 0 \quad 0\ ]^T$	deg
Control Torque Bound	$\mathbf{u}_{\text{m}}$	$\begin{bmatrix} 9\times10^{-5} & 9\times10^{-5} & 9\times10^{-5} \end{bmatrix}^T$	$\text{N}\cdot\text{m}$
Upper Limit of Wheel Speed	Ω_{U}	2000	rpm
Lower Limit of Wheel Speed	Ω_{L}	1800	rpm
Lower Speed of All Wheels	Ω_{AL}	100	rpm
Proportional Gain	K_p	diag(0.5, 0.5, 0.5)	–
Derivative Gain	K_d	diag(10, 10, 10)	–
Sample Time	T	0.25	s

actual controller of the ZDPS-2. The wheel speeds in the RWA are shown in Fig. 8. The disturbance torque are shown in Fig. 9. As can be seen, from time 5000 s to time 10000 s, the wheel speed changes are up to 6000 rpm, and the torques reach up to 4 mN · m. The attitude errors are about 6° as shown in Fig. 10.

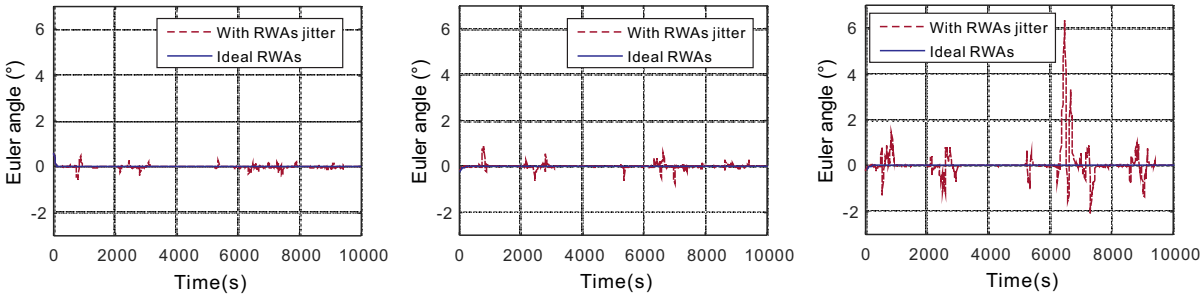

(a) Rotation X Axis **(b) Rotation Y Axis** **(c) Rotation Z Axis**

Fig. 7 The jitter effects on the Euler angles.

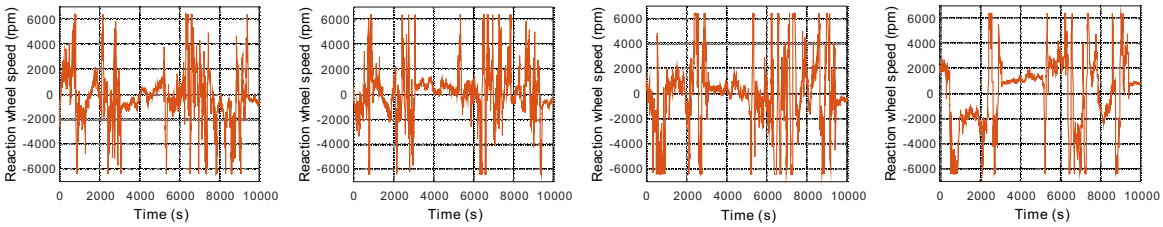

(a) RW1 **(b)** RW2 **(c)** RW3 **(d)** RW4

Fig. 8 Reaction wheel speed histories with PD controller.

Then, the adaptive moment distribution algorithm is added to the PD controller. As shown in Fig. 11, the speeds of the RWs are significantly reduced and the vibration torque is thus suppressed, as shown in Fig. 12. As a result, the attitude error angle is less than 0.1° now, as shown in Fig. 13. The SMC controller is used alone as a comparison. At about time 6000 s, the attitude error is about 6°, as seen in Fig. 16. Also, note its control effect is similar to that of the PD controller. The speeds of the RWA wheels reach 6000 rpm, as shown in Fig. 14. Also, RWA jitter disturbance torques are up to 4 mN · m, as shown in Fig. 15, exceeding the maximum torque that the RWA can implement. Obviously, this could not satisfy the control system requirements.

As shown in Figs. 17 – 19, when combining the SMC controller with the adaptive momentum distribution algorithm, the overall accuracy is improved significantly. The wheel speed is limited to the 2000 rpm, and the jitter effects of the wheel speeds are gradually diminishing. The jitter torque is limited in 0.05 mN · m. Thus the stability conditions of the controller are satisfied. The attitude error is smaller than 0.001°. Therefore, the effect of RWA jitter on the micro-satellite attitude is significantly reduced.

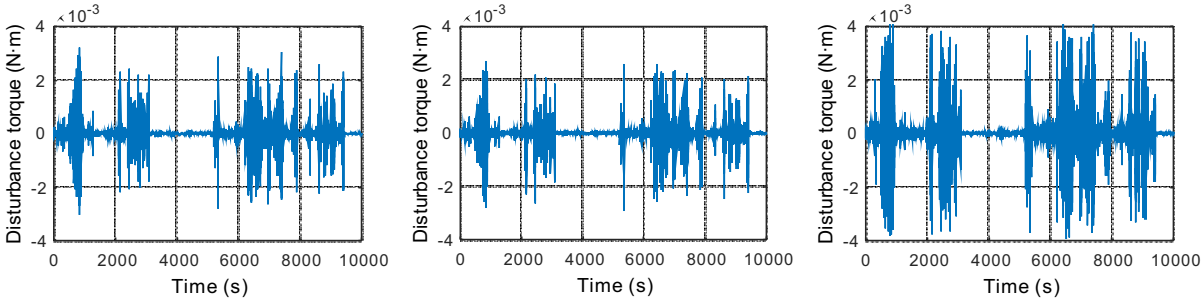

(a) Rotation X Axis (b) Rotation Y Axis (c) Rotation Z Axis

Fig. 9 Reaction wheel disturbance torques with PD controller.

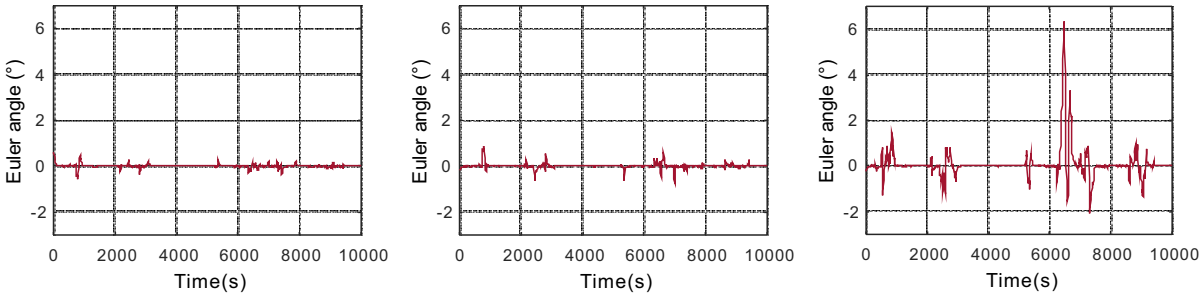

(a) Rotation X Axis (b) Rotation Y Axis (c) Rotation Z Axis

Fig. 10 Euler angle histories with PD controller.

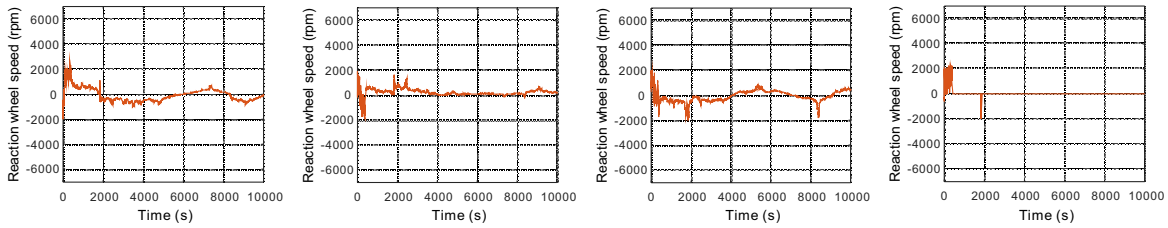

(a) RW1 (b) RW2 (c) RW3 (d) RW4

Fig. 11 Reaction wheel speed histories with PD controller and adaptive moment distribution algorithm.

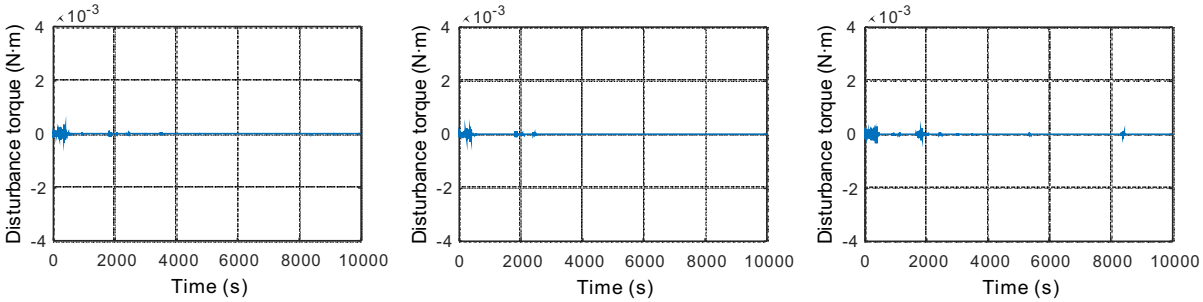

(a) Rotation X Axis (b) Rotation Y Axis (c) Rotation Z Axis

Fig. 12 Reaction wheel disturbance torques with PD controller and adaptive moment distribution algorithm.

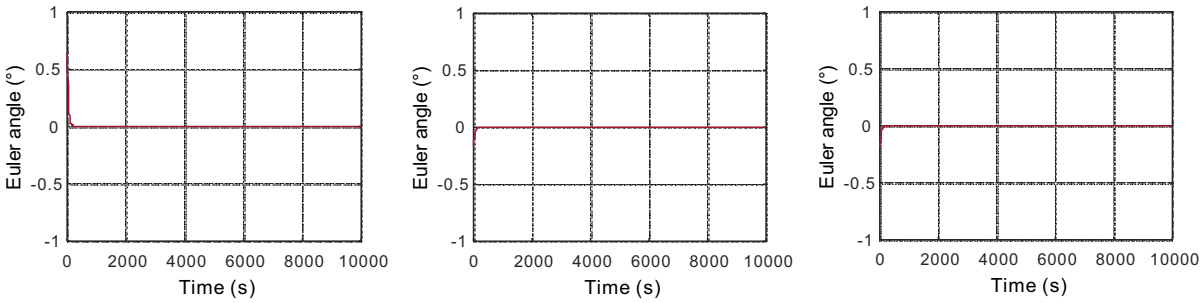

(a) Rotation X Axis **(b) Rotation Y Axis** **(c) Rotation Z Axis**

Fig. 13 Euler angle histories with PD controller and adaptive moment distribution algorithm.

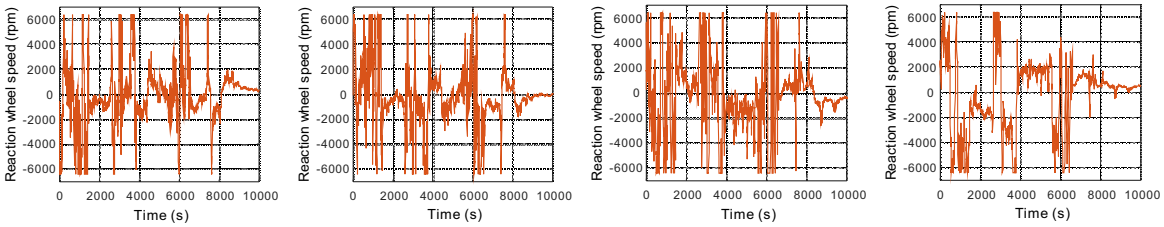

(a) RW1 **(b)** RW2 **(c)** RW3 **(d)** RW4

Fig. 14 Reaction wheel speed histories with SMC controller.

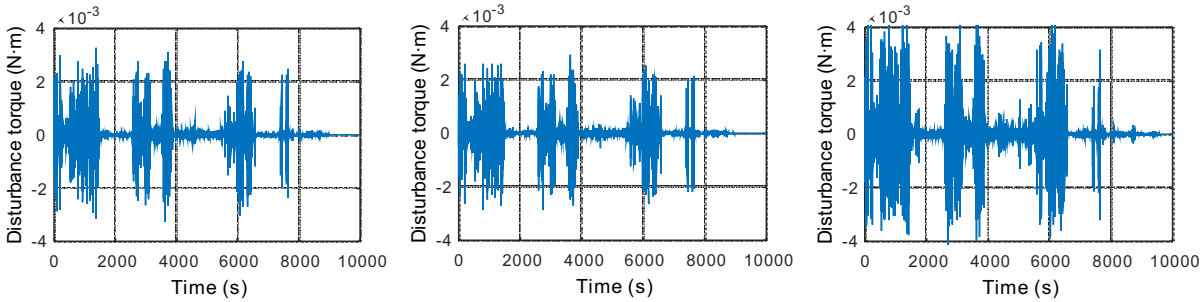

(a) Rotation X Axis **(b) Rotation Y Axis** **(c) Rotation Z Axis**

Fig. 15 Reaction wheel disturbance torques with SMC controller

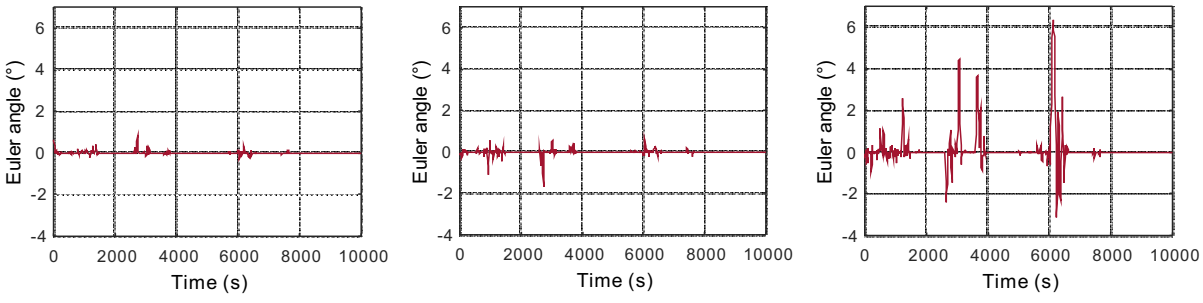

(a) Rotation X Axis **(b) Rotation Y Axis** **(c) Rotation Z Axis**

Fig. 16 Euler angle histories with SMC controller.

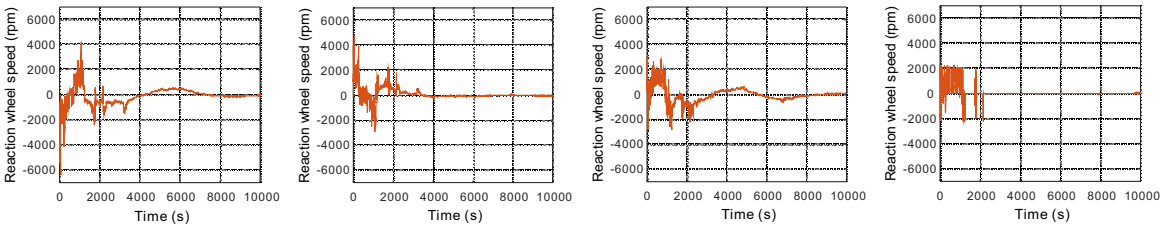

(a) RW1 **(b)** RW2 **(c)** RW3 **(d)** RW4

Fig. 17 Reaction wheel speed histories with SMC controller and adaptive momentum distribution algorithm.

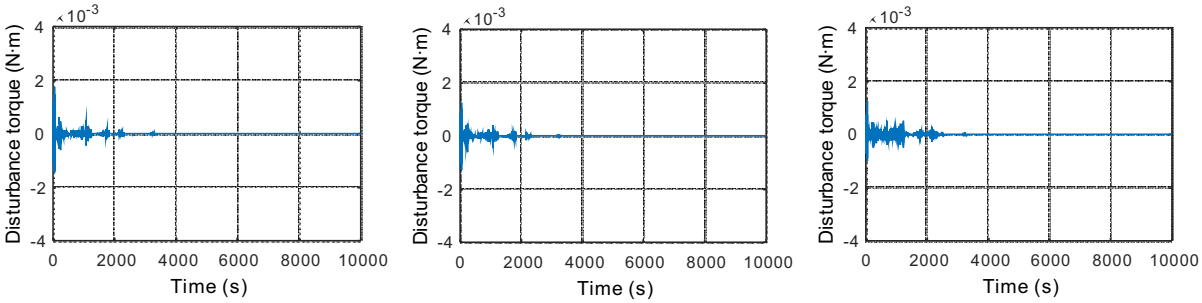

(a) Rotation *X* Axis **(b) Rotation *Y* Axis** **(c) Rotation *Z* Axis**

Fig. 18 Reaction wheel disturbance torques with SMC controller and adaptive moment distribution algorithm.

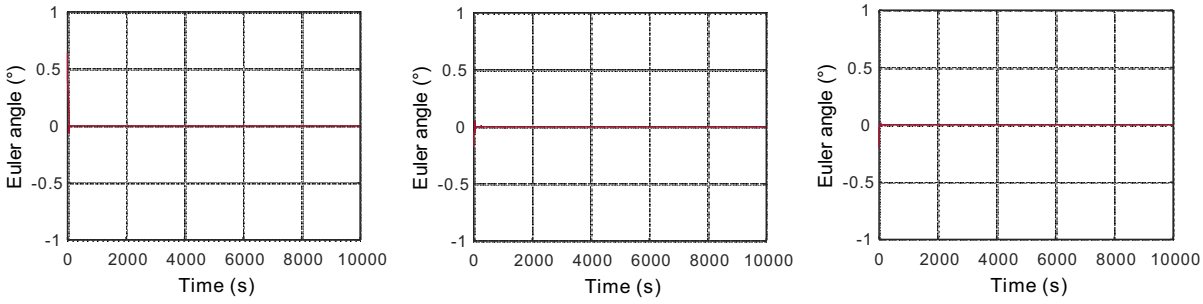

(a) Rotation *X* Axis **(b) Rotation *Y* Axis** **(c) Rotation *Z* Axis**

Fig. 19 Euler angle histories with SMC controller and adaptive momentum distribution algorithm.

V. Conclusions

Reaction wheel assembly (RWA) jitter disturbances may not be able to be ignored when designing a high precision micro-satellite. As shown in a typical application of a real micro-satellite, the RWA jitter itself can attribute about 6° error in the attitude pointing. When a RWA's full model is adapted to the micro-satellite attitude control system, it shows that compared with its previous precision of 6°, with the use of an adaptive torque distribution control logic, a proportional-derivative controller can achieve an attitude precision of 0.1°, while the sliding mode controller combined with the adaptive momentum distribution can reduce the error to 0.001°. This indicates that the RWA jitter interference can been effectively reduced. The adaptive torque distribution control law is simple to implement, and it can be used in combination with most controllers. Thus, it is a viable method in designing a high-precision control system for micro-satellites.

References

[1] Kahr, E., Montenbruck, O., and O'Keefe, K. P. G., "Estimation and Analysis of Two-Line Elements for Small Satellites," *Journal of Spacecraft and Rockets*, Vol. 50, No. 2, 2013, pp. 433–439. doi:10.2514/1.A32352.

[2] Spangelo, S., and Longmier, B., "Optimization of CubeSat System-Level Design and Propulsion Systems for Earth-Escape Missions," *Journal of Spacecraft and Rockets*, Vol. 52, No. 4, 2015, pp. 1009–1020. doi:10.2514/1.A33136.

[3] Hudson, J., Spangelo, S., Hine, A., Kolosa, D., and Lemmer, K., "Mission Analysis for CubeSats with Micro propulsion," *Journal of Spacecraft and Rockets*, Vol. 53, No. 5, 2016, pp. 836–846. doi:10.2514/1.A33564.

[4] Watanabe, H., Masuda, K., and Uchiyama, K., "Satellite Attitude Control System Using Three-Dimensional Reaction Wheel," *AIAA Guidance, Navigation, and Control Conference, AIAA SciTech Forum*, AIAA, 2015, AIAA 2015-1782. doi:10.2514/6.2015-1782.

[5] Louke, J. A., Schmidt, E. S., and Young, C. J., "An Open-Source Reaction Wheel System for Oregon's First Satellite," *AIAA SPACE 2016, AIAA SPACE Forum*, AIAA, 2016, AIAA 2016-5346. doi:10.2514/6.2016-5346.

[6] Katsukawa, Y., Masada, Y., Shimizu, T., Sakai, S., and Ichimoto, K., "Pointing Stability of Hinode and Requirements for the Next Solar Mission Solar-C," *International Conference on Space Optics*, Vol. 10565, The International Society for Optics and Photonics, Rhodes, Greece, 2017, pp. 10565 – 10565 – 6. doi:10.1117/12.2309171.

[7] Rizzo, M. J., Rinehart, S. A., Alcorn, J. B., Barclay, R. B., Barry, R. K., Benford, D. J., Dhabal, A., Fixsen, D. J., Gore, A. S., Johnson-Shapoval, S., Leisawitz, D. T., Maher, S. F., Mundy, L. G., Papageorgiou, A., Pascale, E., Rau, A., Silverberg, R. F., Taraschi, P., Veach, T. J., and Weinreich, S., "Building an Interferometer at the Edge of Space: Pointing and Phase Control System for BETTII," Proceedings of SPIE, Montreal, Quebec, Canada, 2014. doi:10.1117/12.2055016.

[8] Remedia, M., Aglietti, G. S., and Richardson, G., "A Stochastic Methodology for Predictions of the Environment Created

by Multiple Micro Vibration Sources," *Journal of Sound and Vibration*, Vol. 344, February, 2015, pp. 138–157. doi: 10.1016/j.jsv.2015.01.035.

[9] Remedia, M., Aglietti, G. S., Richardson, G., and Sweeting, M., "Integrated Semi Empirical Methodology for Micro Vibration Prediction," *AIAA Journal*, Vol. 53, No. 5, 2015, pp. 1236–1250. doi:10.2514/1.J053339.

[10] Topland, M. P., and Gravdah, J. T., "Nonlinear Attitude Control of the Micro Satellite ESEO," *55th International Astronautical Congress of the International Astronautical Federation, the International Academy of Astronautics, and the International Institute of Space Law*, AIAA, 2004. doi:10.2514/6.IAC-04-A.P.12.

[11] Gross, K., Hoffman, J., Clark, M., Swenson, E., Cobb, R., Whalen, M., and Wagner, L., "Evaluation of Formal Methods Tools Applied to a 6U CubeSat Attitude Control System," *AIAA SPACE 2015 Conference and Exposition, AIAA SPACE Forum*, AIAA, 2015, AIAA 2015-4529. doi:10.2514/6.2015-4529.

[12] Gross, K. H., Patrick, R., Swenson, E., and Agte, J. S., "Optimal Attitude Control of a 6U CubeSat with a Four-Wheel Pyramid Reaction Wheel Array and Magnetic Torque Coils," *AIAA Modeling and Simulation Technologies Conference, AIAA SciTech Forum*, AIAA, 2016, AIAA 2016-0174. doi:10.2514/6.2016-0174.

[13] Kjellberg, H. C., and Lightsey, E. G., "Discretized Constrained Attitude Pathfinding and Control for Satellites," *Journal of Guidance, Control, and Dynamics*, Vol. 36, No. 5, 2013, pp. 1301–1309. doi:10.2514/1.60189.

[14] Zavoli, A., De Matteis, G., Giulietti, F., and Avanzini, G., "Single-Axis Pointing of an Underactuated Spacecraft Equipped with Two Reaction Wheels," *Journal of Guidance, Control, and Dynamics*, Vol. 40, No. 6, 2017, pp. 1465–1471. doi: 10.2514/1.G002182.

[15] Han, Y., Biggs, J. D., and Cui, N., "Adaptive Fault-Tolerant Control of Spacecraft Attitude Dynamics with Actuator Failures," *Journal of Guidance, Control, and Dynamics*, Vol. 38, No. 10, 2015, pp. 2033–2042. doi:10.2514/1.G000921.

[16] Inamori, T., Wang, J. H., Saisutjarit, P., and Nakasuka, S., "Jitter Reduction of a Reaction Wheel by Management of Angular Momentum using Magnetic Torquers in Nano- and Micro-satellites," *Advances in Space Research*, Vol. 52, No. 1, 2013, pp. 222–231. doi:10.1016/j.asr.2013.02.014.

[17] Bialke, B., "High Fidelity Mathematical Modeling of Reaction Wheel Performance," *Advances in the Astronautical Sciences*, Vol. 98, 1998, American Astronautical Society 98-063, pp. 483–496.

[18] Masterson, R. A., "Development and Validation of Empirical and Analytical Reaction Wheel Disturbance Models," M.S. Thesis, Massachusetts Institute of Technology, 1999.

[19] Masterson, R., Miller, D., and Grogan, R., "Development of Empirical and Analytical Reaction Wheel Disturbance Models," *40th Structures, Structural Dynamics, and Materials Conference and Exhibit, Structures, Structural Dynamics, and Materials and Co-located Conferences*, AIAA, 1999, AIAA 99-1204. doi:10.2514/6.1999-1204.

[20] Bialke, B., "A Compilation of Reaction Wheel Induced Spacecraft Disturbances," *20th Annual American Astronautical Society Guidance and Control Conference*, American Astronautical Society, 1997. American Astronautical Society 97-038.

[21] Zhang, Z., Aglietti, G. S., and Zhou, W. Y., "Microvibrations Induced by a Cantilevered Wheel Assembly with a Soft-Suspension System," *AIAA Journal*, Vol. 49, No. 5, 2011, pp. 1067–1079. doi:10.2514/1.J050791.

[22] Zhang, Z., Aglietti, G. S., and Ren, W. J., "Coupled Microvibration Analysis of a Reaction Wheel Assembly Including Gyroscopic Effects in its Accelerance," *Journal of Sound and Vibration*, Vol. 332, No. 22, 2013, pp. 5748–5765. doi: 10.1016/j.jsv.2013.06.011.

[23] Addari, D., Aglietti, G. S., and Remedia, M., "Experimental and Numerical Investigation of Coupled Microvibration Dynamics for Satellite Reaction Wheels," *Journal of Sound and Vibration*, Vol. 386, October, 2017, pp. 225–241. doi: 10.1016/j.jsv.2016.10.003.

[24] Addari, D., Aglietti, G. S., and Remedia, M., "Dynamic Mass of a Reaction Wheel Including Gyroscopic Effects: An Experimental Approach," *AIAA Journal*, Vol. 55, No. 1, 2017, pp. 274–285. doi:10.2514/1.J055398.

[25] Peng, C., Fang, J. C., and Cui, P. L., "Dynamics Modeling and Measurement of the Microvibrations for a Magnetically Suspended Flywheel," *IEEE Transactions on Instrumentation and Measurement*, Vol. 64, No. 12, 2015, pp. 3239–3252. doi:10.1109/Tim.2015.2459491.

[26] Wang, H., Han, Q. K., Luo, R. Z., and Qing, T., "Dynamic Modeling of Moment Wheel Assemblies with Nonlinear Rolling Bearing Supports," *Journal of Sound and Vibration*, Vol. 406, June, 2017, pp. 124–145. doi:10.1016/j.jsv.2017.06.019.

[27] Alcorn, J., Allard, C. J., and Schaub, H., "Fully-Coupled Dynamical Jitter Modeling of a Rigid Spacecraft with Imbalanced Reaction Wheels," *AIAA/AAS Astrodynamics Specialist Conference, AIAA SPACE Forum*, AIAA, 2016, AIAA 2016-5686. doi:10.2514/6.2016-5686.

[28] Markley, F. L., and Crassidis, J. L., *Fundamentals of Spacecraft Attitude Determination and Control*, Springer, New York, NY, 2014, pp. 345–359.

[29] Wie, B., and Barba, P., "Quaternion Feedback for Spacecraft Large Angle Maneuvers," *Journal of Guidance, Control, and Dynamics*, Vol. 8, No. 3, 1985, pp. 360–365. doi:10.2514/3.19988.

[30] Wie, B., Weiss, H., and Arapostathis, A., "A Quaternion Feedback Regulator for Spacecraft Eigenaxis Rotations," *Guidance, Navigation and Control Conference*, AIAA, 1988, 88-4128-CP. doi:10.2514/6.1988-4128.

[31] Bošković, J. D., Li, S.-M., and Mehra, R. K., "Robust Adaptive Variable Structure Control of Spacecraft Under Control Input Saturation," *Journal of Guidance, Control, and Dynamics*, Vol. 24, No. 1, 2001, pp. 14–22. doi:10.2514/2.4704.